Journal of Membrane Science 498 (2016) 276–290

Contents lists available at ScienceDirect

Journal of Membrane Science

journal homepage: www.elsevier.com/locate/memsci

Mixed-matrix membranes of zeolitic imidazolate framework (ZIF-8)/Matrimid nanocomposite: Thermo-mechanical stability and viscoelasticity underpinning membrane separation performance

E.M. Mahdi, Jin-Chong Tan *

Department of Engineering Science, Parks Road, OX1 3PJ, University of Oxford, United Kingdom

ARTICLE INFO

Article history:
Received 2 July 2015
Received in revised form
29 September 2015
Accepted 30 September 2015
Available online 9 October 2015

Keywords:
Mixed-matrix membranes
Metal-organic framework (MOF)
Zeolitic imidazolate framework (ZIF)
Nanocomposites
Mechanical stability

ABSTRACT

Mixed-matrix membranes (MMMs) containing nanoporous metal-organic frameworks (MOFs) represent a rapidly expanding class of next-generation membranes, targeting CO_2 capture, gas purification, and novel electrochemical technologies. In this work, we have performed an in-depth study to elucidate the basic mechanical properties underpinning the functional performance of the prototypical ZIF-8/Matrimid® nanocomposite membranes. By adopting the colloidal solution mixing method, we have fabricated membranes with 0–30 wt% ZIF-8 nanoparticles, whose quasi-static, temperature- and time-dependent mechanical characteristics have been established by means of nanoindentation, dynamic mechanical analysis, and large-strain uniaxial tensile measurements. We show that the inclusion of ZIF-8 nanoparticles into Matrimid (a glassy polyimide) controls many important mechanical behaviour, ranging from elastic modulus, yield strength and hardness, to ductility (stretchability), fracture strength and toughness. We identified that annealing (180 °C), despite improving the gas permeability and selectivity of Matrimid-based membranes, could substantially degrade its ductility and fracture toughness, while stabilising small-strain viscoelastic response under dynamic loading. Our results suggest that an annealed $< \sim 10$ wt% ZIF-8/Matrimid MMM would be ideal for practical separation applications, where an optimal combination of mechanical resilience in conjunction with excellent gas permselectivity are the prerequisites.

1. Introduction

Recently the attraction of employing polymeric membranes to afford wide ranging energy- and environmental-oriented applications has reached a new zenith [1–3]. The cost competitiveness underpinning emergent membrane technology [4] combined with the ease of processability and stability of organic polymers makes it a strong contender for many important industrial applications, namely selective gas separations [5,6], pervaporation [7], desalination and water purification [8,9]. In fact, the study of its practical applicability will go a long way into propelling membrane technology to the forefront of commercial applications, owing largely to its promising intrinsic material functions, inert characteristics, and lower overall energy requirements [1,2,4]. However, current implementations of neat polymeric membranes for high-throughput processes suffer from several major drawbacks; for instance, reduced materials performance associated with membrane degradation [10–12], which necessitates its constant replacement or additional structural reinforcement.

There is a rapidly growing body of works demonstrating the huge potential of enhancement in the functional properties of neat polymeric membranes and composite systems, which have been highlighted by several excellent review articles [1,2,4,5]. There are various proposals being made to address the inadequacy of neat polymeric membranes, particularly with regards to improvement in processing techniques [13,14], and through the incorporation of filler phases that could alter the physico-chemical characteristics of polymeric mixtures. Processing methods, such as plasma techniques and surface modifications have been demonstrated to be effective in producing durable membranes that are potentially viable for high-end applications, *e.g.* polymer electrolyte membranes [15], while recent examples of composite systems include introduction of graphene oxide as fillers to polyvinylidene fluoride (GO/PVDF) [16], and iron oxide to polyethersulfone (Fe_3O_4/PES) [17]. These methods produced improved gas separation performance [18], sensory abilities [19], together with reports of the scope to tailor the mechanical properties of novel composite

* Corresponding author.
E-mail address: jin-chong.tan@eng.ox.ac.uk (J.-C. Tan).

http://dx.doi.org/10.1016/j.memsci.2015.09.066
0376-7388/

membranes, including the Young's modulus [20,21], tensile strength [22] and toughness [23].

Although some of the strategies outlined above were successful in enhancing the functional performance of polymeric membranes, other attempts were not, which goes to show that such improvements were not universally achievable. Instead it may be dependent upon specific combinations of polymer matrix, filler inclusion, or processing techniques used [24,25]. Notwithstanding the above, subsequent developments witnessed in emerging fields such as hybrid nanomaterials and fine-scale characterisation techniques promise to address certain core challenges linked to these issues, where the inclusion of nano-sized fillers with improved dispersion may generate a good combination of mechanical [26]. and functional performance [27]. Indeed this is the rationale behind the concept of *nanocomposites* [25], for which the integration of a small quantity of nanofillers into a polymer matrix will result in a marked improvement to the physico-chemical properties of novel polymer-based composites.

Notably, the last decade has witnessed the advent of a revolutionary new class of porous hybrid materials, termed the Metal-Organic Frameworks (MOFs) [28,29]. MOFs are constructed by self-assembly of metal ions/-oxo clusters coordinated by versatile organic linkers, yielding numerous 2-D [30] and 3-D nanoporous compounds, the latter of which typically with an exceptionally high surface area (1000-10,000 $m^2 g^{-1}$) [31]. Of the numerous materials discovered to date [32], Zeolitic Imidazolate Frameworks (ZIFs) [33,34] represent a topical sub-family of MOFs, whose framework structures closely mimicking the diverse topology of inorganic zeolites. While the chemical stability of ZIFs reflects those of zeolites [33], their thermo-mechanical properties [35,36] and structural stability [37,38] are relatively weaker compared to their inorganic counterparts. Nevertheless, given their highly tuneable physico-chemical properties [39], ZIF- and MOF-based "mixed-matrix membranes" (MMMs) [40,41] are at the forefront of novel nanocomposite membrane research, targeting gas separation and purification processes [42,43], pervaporation [44], and electrochemical energy conversion and storage systems [45]. Particularly, the prevalence of organic ligands intrinsic to the framework of ZIFs and MOFs may open up the possibility of bonding with organic sub-groups abundant in macromolecular polymers, yielding a good combination of malleability, durability and stability [46,47]. These advantages work towards making MOFs applicable both in physically and chemically punishing environments, further expanding its possible applications.

MOF nanocomposite membranes exhibit excellent capacity for gas separations. Representative examples include the works of Song *et al.* [48] who fabricated ZIF-8/Matrimid® membranes for pure gas permeation selectivity studies (CO_2, H_2, and N_2), while earlier Ordoñez *et al.* [49] studied the same system but further investigated molecular separation of gas mixtures (H_2/CO_2 and CO_2/CH_4). Both studies have a larger implication to environmental sustainability, where their successes are imperative to the introduction of a lower energy alternative for existing gas separation technology of greenhouse emissions. Recently, Smithet al. [50]. reported the Ti-UiO-66/PIM-1 MMM for the separation of CO_2 from flue gases, while Rodenas *et al.* [51]. combined CuBDC nanosheets and polyimide to form CuBDC@PI MMM towards CO_2/CH_4 separation. These works posited that the formation of MMM *via* the addition of nano-sized MOFs into polymers produced promising improvements; for instance, an ~150% increase in permeability for Ti-UiO-66/PIM-1 MMM (5 wt% loading) was reported as opposed to its neat PIM-1 matrix, accompanied by an increased in separation selectivity of 30-80% *vis-à-vis* CO_2/CH_4.

A large proportion of studies reported on MOF-polymer nanocomposites are concerned with the functional performance alone, focusing predominantly on selective adsorption and diffusion properties that govern the permselectivity of MMMs [6,42,52]. In contrast, we note that the corresponding studies pertaining to either the mechanical properties or the thermo-mechanical stability of MMMs, hitherto, remain remarkably scarce [40]. It is imperative that the mechanical, thermal, and (time-dependent) viscoelastic properties of MOF-based MMMs be studied in greater detail, because a comprehensive understanding of these physical properties will enable prediction, rational design and engineering of bespoke materials for practical applications. To this end, the motivation of this paper is to address some of the shortcomings pinpointed above, particularly by means of a systematic thermo-mechanical study performed on a prototypical Matrimid-based MMM—ZIF-8/Matrimid® nanocomposite, which is a promising candidate for H_2/CH_4, H_2/N_2 and CO_2/CH_4 separations [48,49]. Importantly also, this work represents the first definitive study elucidating the structure-mechanical property correlations of a prototypical MOF-polymer MMM, whereby the methodologies developed herein can be adopted to characterise a broad range of existing and upcoming MOF-based membrane systems [52].

2. Materials & methods

2.1. Synthesis of metal-organic framework (MOF) nanoparticles: ZIF-8

Nanoparticles of ZIF-8 shown in Fig. 1(a) were prepared in accordance to the previously reported room-temperature rapid

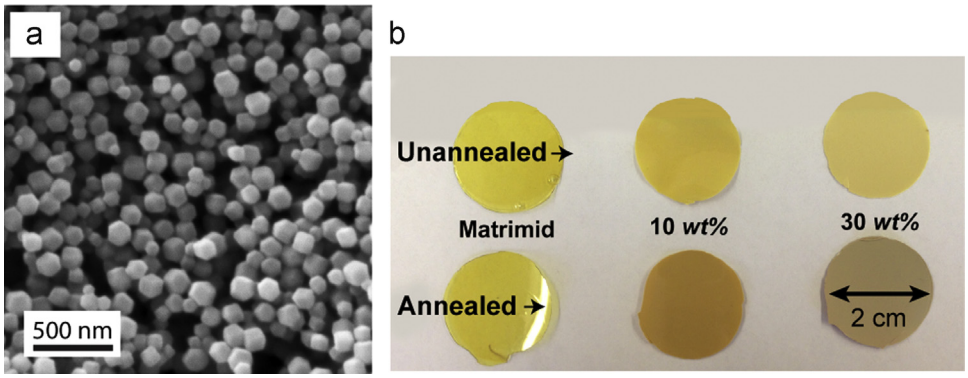

Fig. 1. (a) SEM image showing ZIF-8 nanoparticles prepared by rapid synthesis at room temperature. The mean size of nanoparticle is 147 ± 7 nm (standard deviation derived from 60 measurements from three separate batches). (b) ZIF-8/Matrimid nanocomposite mixed-matrix membranes prepared by colloidal-based solution mixing approach [48], followed by casting via doctor-blade technique. Shown here are unannealed (cured at 60 °C) and annealed (180 °C) membranes, where samples containing ZIF 8 turned opaque upon annealing.

synthesis method [53]. 2.61 g of $Zn(NO_3)_2 \cdot 6H_2O$ and 5.74 g of 2-methylimidazole (purchased from Fisher Scientific and used as is without any further purification) were dissolved in 87 ml of methanol, respectively. The solutions were then mixed into a single beaker and vigorously stirred for an hour, forming a milky white solution after a few minutes. The resulting ZIF-8 nanoparticles were then separated from the solution *via* centrifugation at 8000 rpm for 10 min, and then (without drying) re-dispersed as a colloidal suspension in chloroform ($CHCl_3$).

2.2. Fabrication of ZIF-8/Matrimid mixed-matrix membranes (MMMs)

The Matrimid polymer solution was prepared by dissolving Matrimid® 5218 powder (a fully imidized thermoplastic polyimide supplied by Huntsman Corporation) in chloroform for a total of 24–48 h, until the flakes were visually determined to have completely dissolved in the chloroform-laden solution. Subsequently, the previously synthesised ZIF-8 nanoparticles dispersed as colloids were added in stages to the Matrimid solution, corresponding to the wt% equation below:

$$\text{ZIF–8 } wt.\,\% = \left(\frac{m_{\text{ZIF–8}}}{m_{\text{ZIF–8}} + m_{\text{Matrimid}}}\right) \times 100\% \quad (1)$$

where $m_{\text{ZIF-8}}$ is the weight of the ZIF-8 nanoparticles dispersed in chloroform, and m_{Matrimid} is the weight of the Matrimid flakes dissolved in chloroform. This results in the production of three distinct samples of nanocomposite mixed-matrix membrane (MMM), featuring varied ZIF-8 loadings (Fig. 1(b)): 10, 20, and 30 wt%, respectively. Importantly, recent work by Song *et al.* [48] confirmed that the application of this *colloidal solution mixing* approach may significantly reduce the danger of nanoparticle agglomeration, otherwise witnessed in MMMs produced by re-dispersion of dried ZIF-8 nanoparticles [49].

To create membranes depicted in Fig. 1(b), the ZIF-8/Matrimid MMM solutions were cast using an automatic doctor-blade coater (MTI Corp. AFA-II) at a constant speed of 10 mm s^{-1} onto a glass substrate, resulting in an average thickness of 145 ± 7 μm for each membrane. The resultant membranes were then transferred to a glove bag saturated with chloroform vapour, and left to slow-cure for 24 h, after which they were removed from the glove bag and placed in a vacuum oven, and cured for an additional 24 h at 60 °C. After 24 h, the membranes were detached from the glass substrate (by submerging in water) and stored for subsequent studies; another set of membranes, however, was further annealed for 24 h at 180 °C under vacuum. As such two sets of membranes, *i.e.* 'un-annealed' (cured at 60 °C) and 'annealed' (cured at 180 °C) have been prepared for this study.

2.3. Materials characterisation

The following characterisation methods were chosen for their respective capabilities to determine the morphological, mechanical, thermal, and viscoelastic properties of the ZIF-8/Matrimid® membranes.

Cross-sectional morphology of the MMM was examined using the Scanning Electron Microscope (TESCAN LYRA3 FEG-SEM/FIB apparatus). The membrane samples were immersed and fractured in a bath of liquid nitrogen (LN_2 at 77 K) and mounted at a 90° angle on a stub using adhesives, exposing the through-thickness surface. Each sample was coated with gold using a sputter coater for a period of 30 seconds, prior to imaging at 15 kV under high vacuum.

Atomic force microscopy (AFM) surface characterisation was conducted using the MFP-3D AFM (Asylum Research, Oxford Instruments) in tapping mode using the AC-air topography settings. The samples, each measuring 5×10 mm^2, were mounted on stainless steel coupons (using carbon tapes and adhesives) to reveal the top surface of membranes.

X-ray diffraction (XRD) was conducted using the Rigaku-2250 setup, operating at 45 kV and a tube current of 200 mA using the CuKα source (1.5418 Å). The scanning rate was set to 0.5 min^{-1} with a continuous scanning range of $2\theta = 5$–30°.

The thermal stability and decomposition was investigated using the TGA-Q50 (TA Instruments), equipped with an induction heater (maximum temperature of 1000 °C) and a platinum sample holder. Samples weighing an average of 4 mg were loaded onto the sample holder and the samples were heated from 50 to 1000 °C at a rate of 10 °C min^{-1}, to the point of complete decomposition. The data was collected and plotted using the TA Analyser software.

2.4. Thermo-mechanical properties characterisation

Temperature-dependent viscoelastic measurements were performed using the TA Instruments Q800 Dynamic Mechanical Analyser (DMA) equipped with an LN_2 attachment. The dynamic experiments were performed at a heating rate of 3 °C min^{-1} from −100 to 400 °C. The DMA was calibrated to a pair of tension film clamps and fixed to a gauge length of 12.5 mm, with all samples tested under uniaxial tensile mode. The static force was at 0.1 N with the force track set to 125%. The multi-frequency sweep setting was applied, where the oscillating frequency was cyclically alternating between 5,10,15,20, and 25 Hz as the temperature was increased throughout the experiments.

Quasi-static nanomechanical properties, particularly the Young's modulus (E) and indentation hardness (H) were determined *via* nanoindentation experiments using the MTS NanoIndenter XP (Agilent Technologies, USA), equipped with a Berkovich three-sided pyramid diamond tip. We made a series of 20 indentations in a rectangular configuration for each sample being probed (three membranes tested per wt%).

The stress–strain curves were measured using the Instron universal testing machine (Model 5582), equipped with a 100 N load cell. The width and gauge length of the test coupons were 5 mm and 30 mm, respectively. The samples were clamped to the rigs, and were subjected to a tensile load applied at 0.5 mm min^{-1} until fracture. The load–displacement data obtained were converted to nominal stress–strain plots, using the initial cross-sectional area and gauge length of the samples.

3. Results and Discussion

3.1. Microstructural features of ZIF-8/Matrimid nanocomposite mixed-matrix membranes

Figs. 2 and 3 present SEM images revealing the representative microstructures observed at the cross section of the membranes. It can be seen that there is excellent dispersion and homogeneity of ZIF-8 nanoparticles embedded within the Matrimid polymer matrix. However, the lower loadings of ZIF-8 nanoparticles (~10 wt%) appear to produce a better overall dispersion and blending of ZIF-8, as opposed to those incorporating higher loadings. Despite the use of the solution mixing approach [48] we found evidence of some agglomeration and aggregation of nanoparticles, which becomes more pronounced for the higher loaded membranes, especially those featuring ~30 wt% of ZIF-8. This observation indicates that there is an optimal wt% loading for the blending of Matrimid and ZIF-8 nanoparticles, where both phases could be seamlessly integrated. In fact, the rhombic dodecahedron

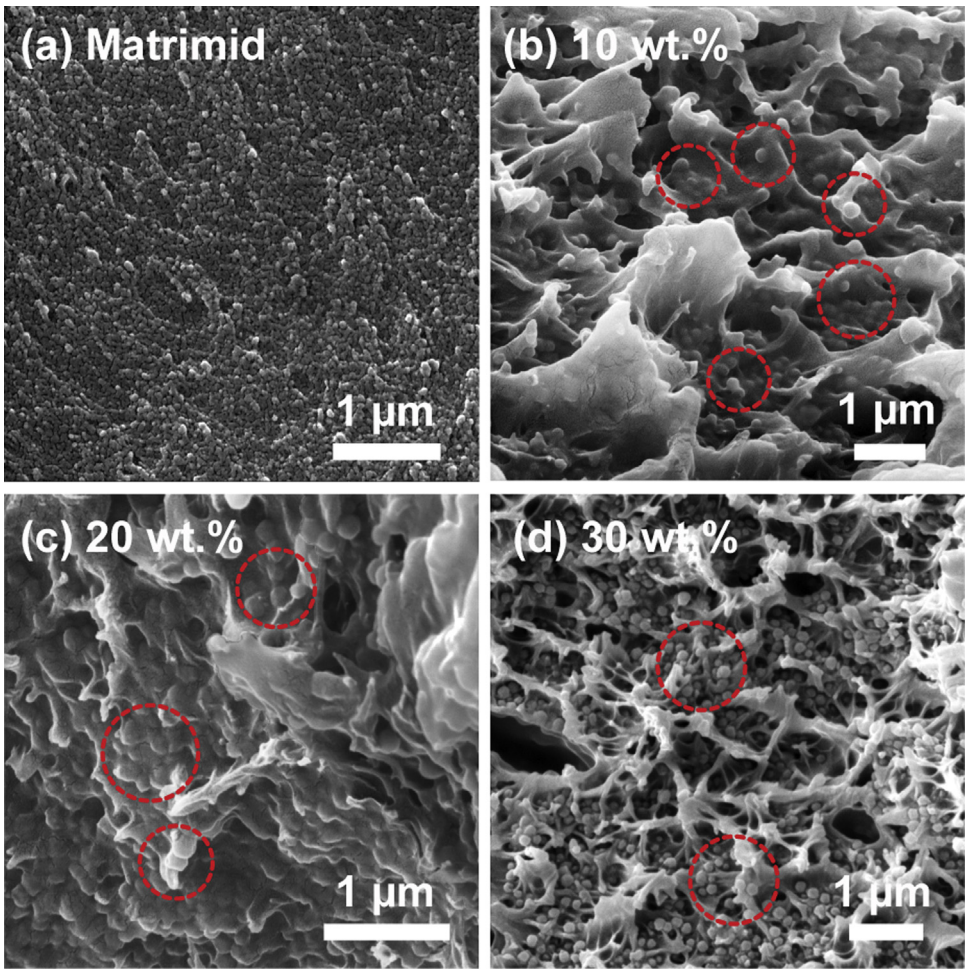

Fig. 2. SEM cross-sectional microstructures of ZIF-8/Matrimid MMM unannealed samples (cured at 60 °C), showing (a) Matrimid, (b) 10 wt%, (c) 20 wt%, and (d) 30 wt% of ZIF-8 nanoparticles. Red markers indicate representative areas where the polymer-encapsulated ZIF-8 nanoparticles are visible. (For interpretation of the references to color in this figure legend, the reader is referred to the web version of this article.).

crystallographic habit [54]. characteristic of ZIF-8 is indistinguishable from the micrographs (see Supplemental Information (SI), Figs. S1, S2), confirming that the nanoparticles are indeed very well encapsulated (by a thin layer of Matrimid) and assumed an approximately spherical shape, which is energetically more favourable [55].

Here it is worthy to emphasise that the micron-sized cavities and pores visible in the SEM images (Fig. 2b) are reminiscent of the classic 'cup-and-cone' ductile fracture mode, as the cross-sectional samples were prepared by the freeze-and-fracture technique in an LN_2 medium. Interestingly, the SEM micrographs reveal that the membranes actually experienced a reasonable degree of ductile failure at the microscopic length scale under 77 K. In light of this, we may infer that ZIF-8 nanoparticles embedded in Matrimid disrupt the molecular packing of the polymeric chains; while this effect improves the overall gas permeability [48], it also gives rise to microscopic defects acting as *stress risers* [46] that are susceptible to localised deformation under load.

The microstructures of the annealed membranes are shown in Fig. 3. Similar to the unannealed membranes, higher loadings demonstrate increasing agglomeration and aggregation, as evidenced by the close packing and prominence of ZIF-8 nanoparticles within the membranes, reminiscent of the microstructures found in the unannealed membranes (Fig. 2). The primary difference between the unannealed and annealed membranes is that the trapped solvents within ZIF-8 and Matrimid have been completely evacuated, as the annealing temperature of 180 °C is substantially higher than the boiling point of chloroform (~60 °C), which is the solvent used for materials processing. Moreover, Matrimid undergoes secondary relaxation (β) at 80–90 °C [56], leading to the molecular stretching of the polymer bonds accompanied by rotations of the side groups, both of which help in accelerating the removal of chloroform. As a consequence of annealing, the fracture surfaces in Fig. 3 suggest that a predominantly brittle failure mechanism is at play, where relatively fewer ductile deformation events can be identified, particularly at higher wt% loadings.

Fig. 4 shows the AFM images acquired from the vicinity of the top surface of the unannealed and annealed membranes, respectively. Both sets of samples exhibit distinctive height topography, which can be linked to the embedded nanoparticles and the corresponding wt%. Nominally, the size of the protruding topographic features lies in the range of 150–200 nm across, thereby consistent with Matrimid-coated ZIF-8 nanoparticles, for which the size of the as-synthesised nanoparticles is relatively smaller, see Fig. 1(a). Therefore it is clear that ZIF-8 is not only embedded inside the membrane (as revealed by SEM cross sections, Figs.2 and 3), but also present near the top subsurface layers, suggesting that a homogeneous dispersion of nanoparticles was achieved throughout the matrix.

Our SEM and AFM studies highlight the presence of a complex microstructure that stems from the two major composite constituents: ZIF-8 and Matrimid. It is envisaged that the multiple phases in the mixed-matrix membrane react differently to

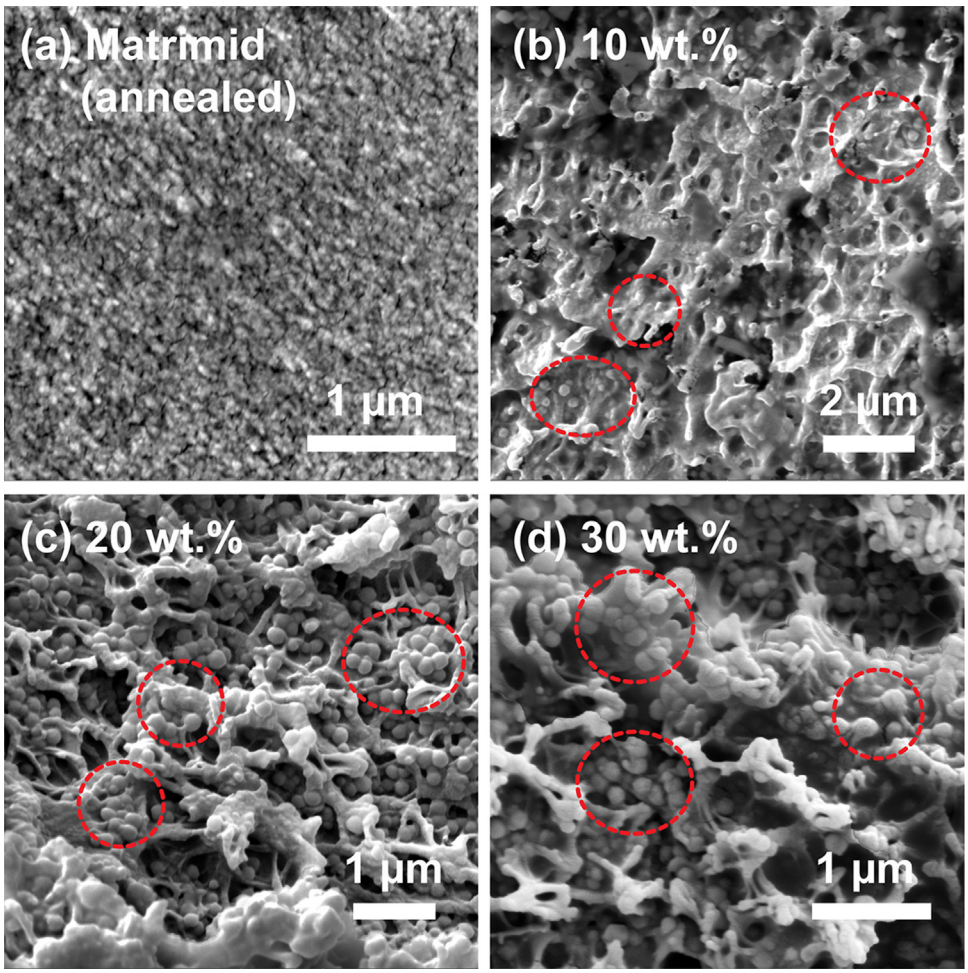

Fig. 3. SEM cross-sectional morphology of ZIF-8/Matrimid MMM subjected to an annealing heat treatment at 180 °C in vacuum. (a) Matrimid, (b) 10 wt%, (c) 20 wt%, and (d) 30 wt% ZIF-8 nanoparticles. Red markers highlight the presence of the polymer-encapsulated nanoparticles. (For interpretation of the references to color in this figure legend, the reader is referred to the web version of this article.).

external stimuli, such as pressure and/or temperatures, creating stress risers and temperature gradients alongside competing responses within the membrane, all of which underpinning the mechanical performance of MMMs. On this basis, information on mechanical properties, ranging from elastic modulus and yield strength to viscoelasticity, toughness and ductility, and how they change with temperature will prove to be important to enable a wide range of challenging technological implementations [40,42,52].

3.2. Quasi-static mechanical properties determined from nanoindentation studies

Fig. 5 summarises the nanoindentation results obtained from the unannealed and annealed nanocomposite membranes. Using the indentation load-displacement raw data (Fig. S6 in SI), we have determined the Young's modulus (E) of the membranes, assuming an isotropic response, in accordance with the Oliver & Pharr method [57]:

$$\frac{1}{E_r} = \frac{1-\nu^2}{E} + \frac{1-\nu_i^2}{E_i} \quad (2)$$

where E_r is the reduced modulus (derived from contact stiffness recorded by indenter) [58], and E_i and ν_i are Young's modulus and Poisson's ratio of the diamond indenter tip (*i.e.* 1141 GPa and 0.07, respectively); we let the Poisson's ratio of the sample (ν) to be ~0.2. In the case of heterogeneous materials [59], the magnitude of E determined above is representative of the *relative stiffness* [60]. of samples subject to an elastic deformation (fully reversible). On the other hand, the indentation hardness (H) provides a measure of the structural resistance of the membranes against any plastic deformation (irreversible), which is defined by [57]:

$$H = \frac{P}{A_c} \quad (3)$$

where P is the normal indentation load and A_c is the contact area established by the indenter tip under that applied load.

First we will consider the nanoindentation results of unannealed membranes. Intriguingly, it can be seen that the Young's modulus (E) property (Fig. 5a) is inversely proportional to the ZIF-8 nanoparticle content, although their hardness (H) response (Fig. 5b) is demonstrating an upward trend. At 30 wt%, the stiffness of the unannealed membrane decreased by ~8% with respect to the E of neat Matrimid, while the annealed membrane decreased by ~7%. Conversely, the H of the unannealed membrane increased by ~5%, while the annealed membrane increased by ~8%. In fact, we could elucidate this counterintuitive phenomena by invoking the simple Rule of Mixtures (RoM)—the Voigt and Reuss models [61], which respectively predicts the upper- and lower-bounds of E and H values on the basis of the volume-fraction-weighted contributions of the composite constituents. Herein for the RoM calculations, we take for ZIF-8 nanoparticles: $E_{ZIF\text{-}8}$=3.3 GPa [35] and $H_{ZIF\text{-}8}$ ~500 MPa [34]; and for neat

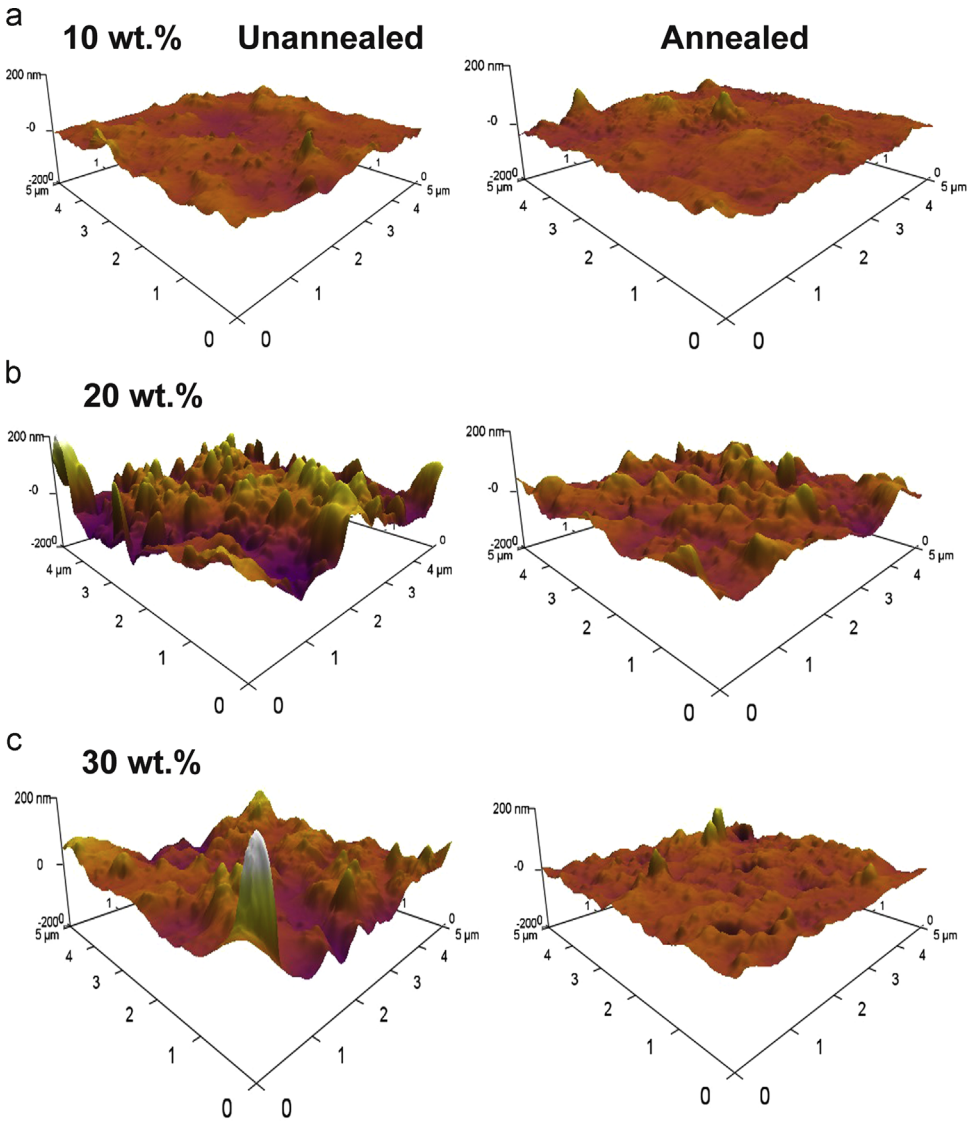

Fig. 4. AFM 3-D scans showing top surface topography of the unannealed (left panel) and the annealed (right panel) ZIF-8/Matrimid MMMs, incorporating (a) 10 wt%, (b) 20 wt%, (c) 30 wt% of ZIF-8 nanoparticles. The regions interrogated by AFM were cross sections made adjacent to top surface.

Matrimid unannealed (Figs. S7 and S8): $E_{Matrimid}$=4 GPa and H_{Matrimid} ~270 MPa [62]. Because $E_{\text{ZIF-8}} < E_{\text{Matrimid}}$, so introducing a higher volume fraction of ZIF-8 into neat Matrimid yields, in effect, a more compliant composite (*i.e.* reduction of E). Given that the differential stiffness of the two constituents is relatively small ($\Delta E/E_{\text{Matrimid}}$ ~0.18), it follows that the deviation between the upper- and lower-bounds of E becomes equally insignificant.

In contrast, we recognise that $H_{\text{ZIF-8}} \gg H_{\text{Matrimid}}$ (specifically, hardness of ZIF-8 is about doubled that of neat Matrimid); the resultant composite therefore exhibits an improvement in hardness due to the higher wt% of ZIF-8. It can subsequently be seen from Fig. 5(b) that the upper bound significantly overestimates the hardness; by comparison, the lower bound (Reuss model) is better at projecting the measured values. This outcome is expected as the Reuss model is derived assuming a non-continuous particulate-based composite system (assuming perfect interfaces), which better resembles the microstructural features seen in the nanocomposites (Fig. 2), though the discrepancies observed might also be associated with imperfections present at the interfaces of nanoparticles and matrix, thus decreasing load transfer.

Turning to the annealed membranes, we established that the abovementioned trends persist. Following the annealing treatment, the magnitudes of elastic modulus and hardness have both increased by up to ~9% and ~18%, respectively. Such a behaviour can be understood by scrutinising the nature of the secondary chemical bonding [63] that exists in the ZIF-8/Matrimid MMM, as illustrated in Fig. 6. We rationalised that the evacuation of entrapped solvent molecules could enhance hydrogen bonding between hydroxyl groups, in conjunction with π–π stacking interactions between the benzene rings that are ubiquitous in the polyimide chains (of Matrimid) and the imidazolates (of ZIF-8). It is anticipated that such combined molecular effects produce a stiffer and harder, yet more brittle membrane. This is especially evident with annealed membranes at higher wt% loading, for example we found that the 30 wt% membrane cracked immediately upon removal from glove bag after curing for 24 h at room temperature.

3.3. *Viscoelastic properties of as-prepared and annealed nanocomposite membranes*

Viscoelastic properties [65] had always been the staple of mechanical characterisation of a broad range of polymeric materials and soft matter, which demonstrate time- and temperature-

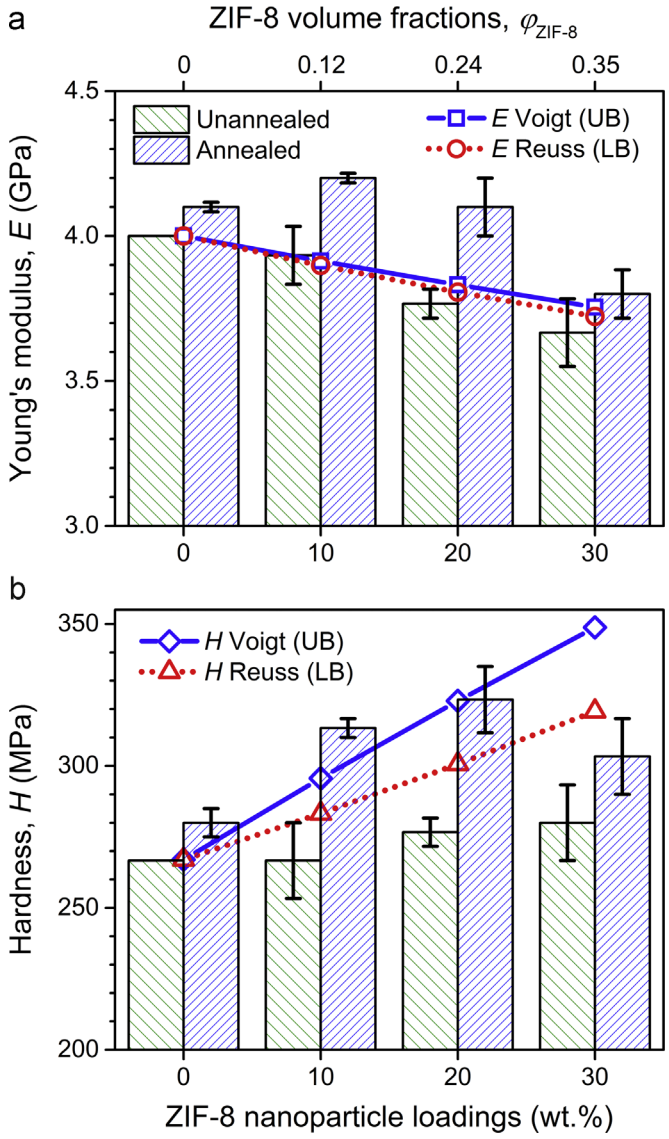

Fig. 5. Nanoindentation data plotted as a function of ZIF-8 nanoparticle loading (in wt% and volume fractions φ_{ZIF-8}), where (a) Young's modulus (E), and (b) nanohardness (H). Each experimental data point corresponds to averaged measurements conducted on three different samples, each subjected to an array of 20 indents to a maximum surface penetration depth of 2 μm. The error bar represents standard deviations derived from 60 individual indents. The upper and lower bounds were computed based on the Rule of Mixture relationships [61], which are expressed in terms of the nanoparticle volume fractions (φ_{ZIF-8}) and elastic moduli or hardness of the composite constituents. The upper bound (UB Voigt) and lower bound (LB Reuss) for Young's modulus of nanocomposites presented in (a) are determined from $E_c = \varphi_{ZIF-8}E_{ZIF-8} + (1-\varphi_{ZIF-8})E_{Matrimid}$ and $E_c = [(\varphi_{ZIF-8}/E_{ZIF-8}) + (1-\varphi_{ZIF-8})/E_{Matrimid}]^{-1}$, respectively. Likewise, the two bounds for hardness in (b) were established using a corresponding set of relationships, where the moduli terms (E's) are substituted by the hardness terms (H's).

dependent mechanical deformation with viscous characteristics. The introduction of nanoparticles (as functional fillers) into polymer matrix and the subsequent modification of viscoelastic response has been the subject of intense interest, with promising results exemplified by a number of recent reports [66–68]. The incorporation of nanoparticles that are structurally and chemically distinct from the polymer matrix phase will induce changes to the matrix, and these changes, however subtle, can be identified *via* the determination of the nanocomposite's viscoelastic properties, *i.e.* the storage and loss moduli (E' and E'', respectively), the loss tangent ($tan\ \delta = E''/E'$) and the accompanying relaxation temperatures [69].

Both the storage modulus (E') and loss modulus (E'') are components of what is termed the *dynamic modulus* (E^*), which can be expressed as [65]:

$$E^* = \frac{\sigma^*}{\varepsilon^*} = E' + iE'' \quad (4)$$

where σ^* and ε^* are the time-varying oscillatory stress and strain, respectively, while $i = \sqrt{-1}$ designating the imaginary component of the loss modulus term E''. The major difference between the Young's modulus (E) and dynamic modulus (E^*) is that, the latter captures the ratio of *dynamic* stress (σ^*) with respect to an oscillatory strain (ε^* adopting a sinusoidal waveform), as opposed to a steadily increasing deformation imposed in the nanoindentation measurements. In the context of MMMs, the storage modulus is representative of the amount of (recoverable) elastic strain energy stored within samples during oscillatory deformation of polymeric chains, whereas the loss modulus corresponds to the amount of energy dissipated through inelastic processes because of entropic motions or rotations of polymeric chains.

The determination of the real and imaginary parts of the dynamic modulus [Eq. (4)] by means of Dynamic Mechanical Analysis (DMA) experiments give us insights into the molecular behaviour of the ZIF-8/Matrimid nanocomposites, as a function of frequency and temperature.

This section will discuss the results garnered from DMA tests and highlight why it is important to study the viscoelastic behaviour of MMMs. Fig. 7 compiles the storage and loss moduli data for the membranes as a function of temperature and nanoparticle wt% loading. We established that the increased addition of ZIF-8 decreased the storage and loss moduli of the membranes before reaching its secondary β-relaxation temperature (80–100 °C). Overall, the order of storage and loss moduli values for the membranes are: Matrimid $>\sim$10 wt% $>$20 wt% $>$30 wt%. However, such differential behaviour becomes negligible upon reaching the primary α-relaxation temperature ($\sim$345 °C) [56], which is known as the glass transition temperature (T_g). It was observed that the introduction of ZIF-8 nanoparticles into Matrimid has an insignificant impact on the T_g of the resulting membranes (Fig. S11). For instance, the variation in T_g between Matrimid and 30 wt% membrane was +0.4% and +0.6% for unannealed and annealed membranes, respectively. Our data show that for temperatures at and beyond T_g, the transition region of the storage and loss moduli of the membranes, whether annealed or not, essentially overlaps one another. Moreover, it was found that in the vicinity of the α-transition ($\sim T_g$), the annealed membranes display relatively higher storage and loss moduli, as shown in Fig. 7(b, d).

The T_g of the membranes can be determined using two approaches; the first, when the storage modulus drops by three orders of magnitude, and the second, when the loss modulus is at its maximum peak. The T_g is clearly visible in Fig. 7, signifying the switch from a (stiff) glassy-to-rubbery (pliant) mechanical response. Notably, we have pinpointed from Fig. 7(c) that the unannealed membranes undergo an additional relaxation when approaching the T_g region, for which we termed ζ-relaxation. The presence of multiple transition peaks is especially striking in the unannealed samples, including neat Matrimid; however, it is absent in all the annealed samples (Fig. 7d).

We have attributed the ζ-transition process to the residual solvent molecules trapped within Matrimid and ZIF-8 nanoparticles, which were only partially removed in curing. During materials processing, ZIF-8 was dispersed in chloroform, while Matrimid flakes were dissolved in chloroform as well. The cage size (11.4 Å, see Fig. 6b) and pore volume (0.485 $cm^3\ g^{-1}$) of ZIF-8 nanoparticles allow for chloroform molecules to enter the porous

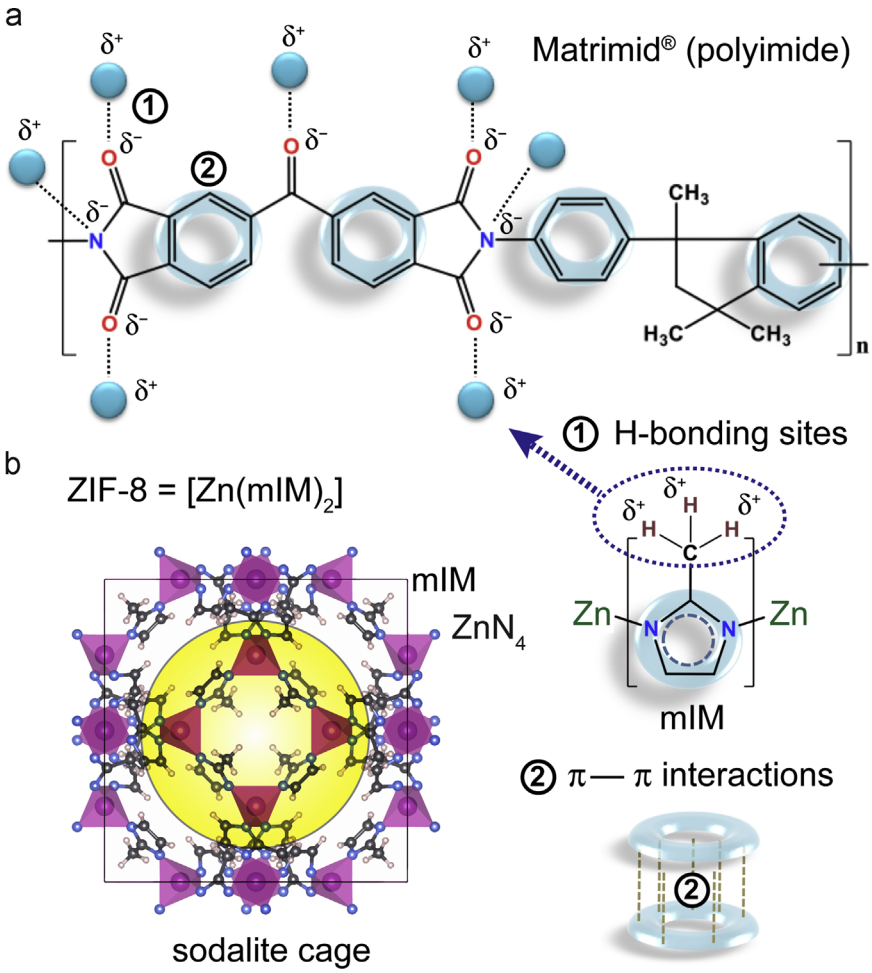

Fig. 6. Schematic illustrating the nature of molecular interactions in the ZIF-8/Matrimid MMM nanocomposite. (a) Polyimide monomer constituting the Matrimid matrix, and (b) ZIF-8, where yellow surface represents the internal porosity (*ca.* 11 Å diameter); *mIM*=[2 methylimidazolate] ligands. Secondary bonding sites comprise hydrogen bonding established by the methyl groups (CH_3) of ZIF-8's organic linkers and the carbonyl and hydroxyl groups prevalent in polyimides, in addition to auxiliary π–π stacking interactions due to delocalised electrons of adjacent benzene rings. The presence of carbonyl and hydroxyl groups in polyimide enables formation of hydrogen bonds [64]. between Matrimid and ZIF-8, giving intimate adhesion between the two constituents. The strength of the H-bonding depends upon the acidity of the proton donor, suggesting that the strength of hydrogen bonds between the aldehyde and methyl group in ZIF-8/Matrimid would be akin to weak interactions such as the *van der Waals* forces. (For interpretation of the references to color in this figure legend, the reader is referred to the web version of this article.).

sodalite cage [34,70], this is facilitated by gate-opening dynamics of the 2-methylimidazolate organic linkers [37]. Solution casting of the membrane will trap solvents within the membrane, and although dried in a vacuum furnace for 24 h at 60 °C (evaporation temperature of chloroform), a small amount of solvents was invariably present, which accounts for the presence of multiple peaks towards the T_g of the unannealed membranes (Fig. 7b). Indeed we have confirmed that annealing the membranes at higher temperatures (180 °C for 24 h) can eliminate the occurrence of ζ-relaxation, endorsed by the presence of only a characteristic peak (α at T_g) for annealed membranes (Fig. 7d). Annealing at a higher temperature (secondary relaxation temperature) initiates bond rotations in polyimides, which could aid in the removal of chloroform trapped within the cages of ZIF-8 nanoparticles bonded to Matrimid by weak interactions (Fig. 6). Approaching T_g, there will be major intermolecular sliding amongst the polyimide chains, freeing trapped chloroform. It is conceivable that the combined movement of Matrimid polymeric chains and the evaporation of chloroform (from pores of Matrimid and cages of ZIF-8) cause major fluctuations in dynamic moduli, resulting in multiple peaks detected near T_g of unannealed membranes.

The presence of multiple peaks and the theory of the evacuation of occluded solvents are further supported with the results from TGA (Fig. S13 and S14), where it is evident that near the T_g, there is a slight weight% decrease in the unannealed membranes, which is attributed to the removal of occluded solvents, due to the fact that this decrease is absent from the annealed membranes. A similar observation has been made on a zeolite/polysulfone membrane system [71]. whereby solvent removal process has been studied using the TGA approach.

Fig. 8 shows the time–temperature superposition (TTS) plots for the storage modulus of the annealed and unannealed membranes. The trends and patterns exhibited by the TTS plots are similar to its storage and loss moduli counterparts. However, the main difference is that the TTS plot enables us to access the behaviour at frequency regions that are either much too high or too low to be practically measured using the DMA test apparatus (limited between 1 and 100 Hz). TTS curves are particularly useful for materials modelling purposes, for example to derive constitutive models for finite-element simulations of engineering components.

3.4. *Large-strain tensile deformation, ductility, and fracture behaviour of membranes*

We performed uniaxial tensile tests to ascertain the mechanical behaviour of the ZIF-8/Matrimid nanocomposite membranes when subjected to a 'large' deformation, *i.e.* exceeding the linear

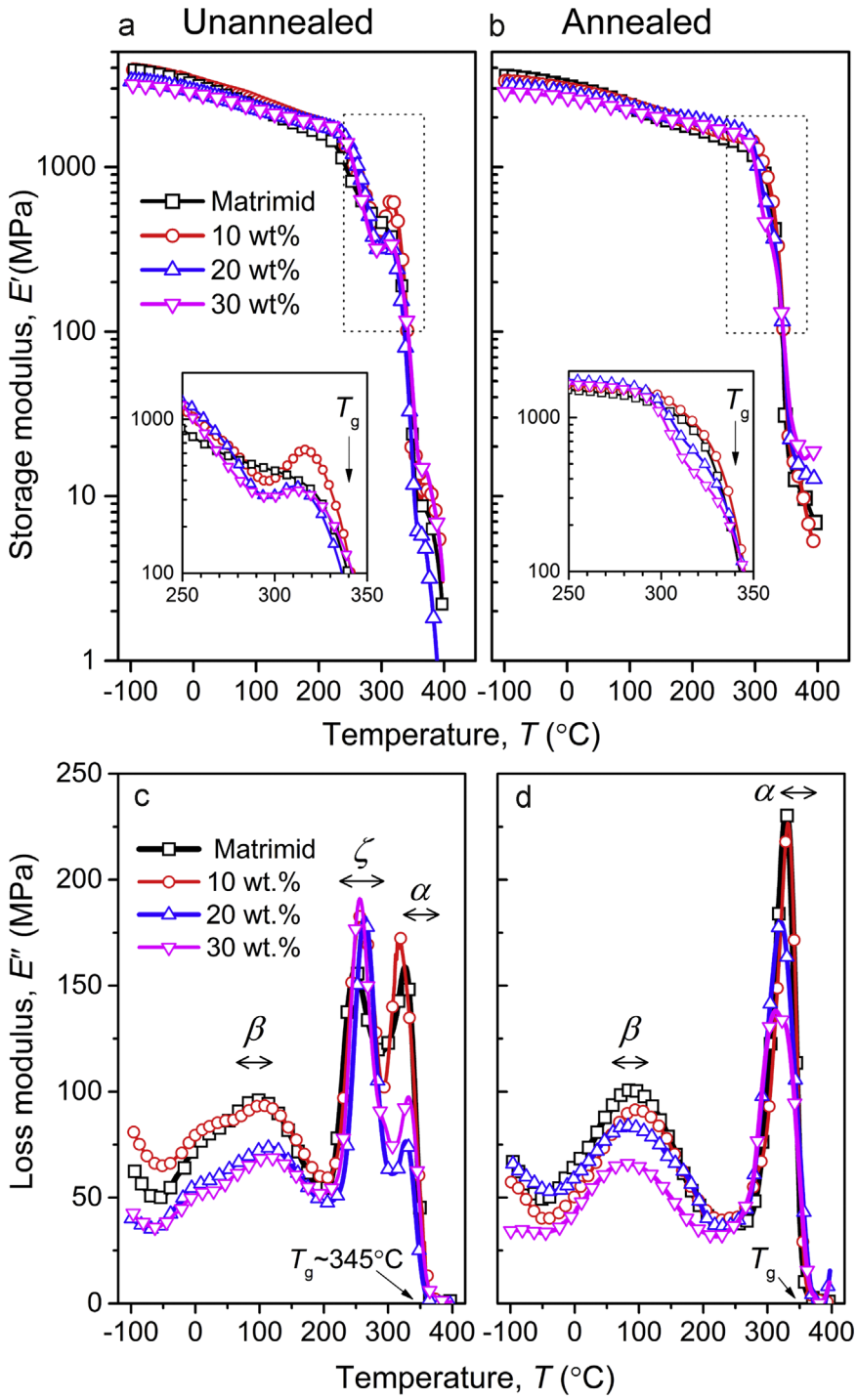

Fig. 7. Storage modulus (E'-top panels, note log scales) and loss modulus (E''-bottom panels) as a function of temperature and ZIF-8 nanoparticle wt% for the (a & c) unannealed, and (b & d) annealed membranes. All DMA measurements were conducted at a frequency of 10 Hz. The insets in (a) and (b) highlight the variations of E' approaching the glass transition temperature, T_g ~345 °C. The primary relaxation is denoted as α, which corresponds to T_g. Secondary relaxations consist of β-transition due to bond rotations in polyimide chains [56], while the ζ-transition identified in this work can be linked to the dynamics linked to the extraction of residual solvent molecules.

elastic limit. Fig. 9(a, b) shows the nominal stress-strain (σ-ε) curves of the unannealed and annealed membranes, respectively, while Fig. 10 summarises the mechanical properties derived from the nominal σ–ε data. Most significantly, it can be seen that the introduction of ZIF-8 nanoparticles into Matrimid resulted in a ductile-to-brittle transition of the resulting membranes. This trend is even more pronounced for the annealed samples, where all, including neat Matrimid, exhibiting appreciably brittle behaviour with an elongation-to-failure (ε_f) that is smaller than ~5%. While neat unannealed Matrimid undergoes substantial strain hardening after yielding (beyond σ_Y ~40 MPa) because of plastic deformation, this trait has been drastically suppressed in annealed membranes due to poor ductility (fast cracking).

We demonstrate that at higher ZIF-8 wt% loading, the membranes are becoming increasingly brittle, and thus vulnerable to cracking and breakage under tension and bending deformation. Likewise, poor ductility is apparent for the annealed membranes, see Fig. 10(a), except for the fact that fracture occurs at a considerably lower strain value compared to the unannealed counterparts. To be able to compare differential membrane toughness

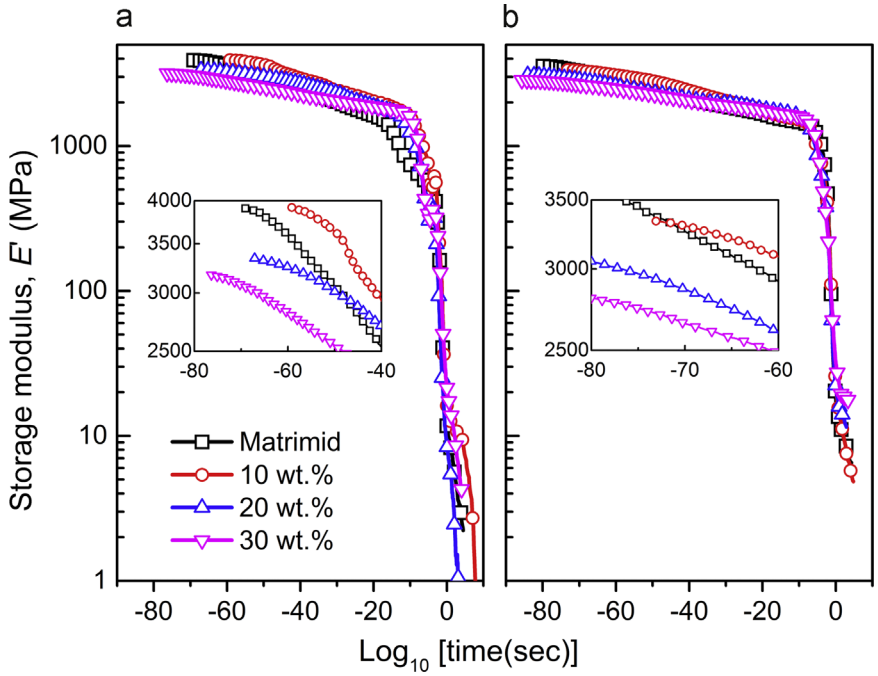

Fig. 8. Time-temperature superposition (TTS) plots for the (a) unannealed and (b) annealed ZIF-8/Matrimid nanocomposite MMMs at reference temperature, T_{ref}=345 °C. The insets show the earlier timescales.

property, herein we propose to characterise the fracture energy (G_f) per unit volume of membrane material, using the following relationship [72], which literally sums up the area encompassed by the σ-ε curves:

$$G_f = \int_0^{\varepsilon_f} \sigma(\varepsilon)\mathrm{d}\varepsilon \tag{5}$$

Fig. 10(b) shows that there is a rapid fall in fracture energy of unannealed membranes as a function of nanoparticle loading. Overall G_f is inversely proportional to both the annealing condition and the nanoparticle loading. In practice, because of a sharp 80–90% decline in fracture energy (thus membrane toughness), the annealed samples with higher ZIF-8 wt% are extremely brittle and easily fractured post-curing. Nevertheless, G_f was found to be relatively comparable for the annealed membranes, suggesting that after the removal of entrapped solvents (and accompanying molecular rearrangements), the large-strain mechanical response of the ZIF-8/Matrimid nanocomposites are controlled by the intrinsically brittle matrix phase, and in principle are becoming less sensitive towards wt% of embedded nanoparticles. Clearly this behaviour is mirrored by ductility (Fig. 10a), where annealing stabilised the values of elongation-to-failure (ε_f), while there is a larger variation determined for the unannealed counterparts.

The yield strength (σ_y) and tensile strength (σ^*) of the unannealed membranes are also strongly affected by the ZIF-8 wt% (Fig. 10c,d). For example, the strengths fell to ~50% level of that of

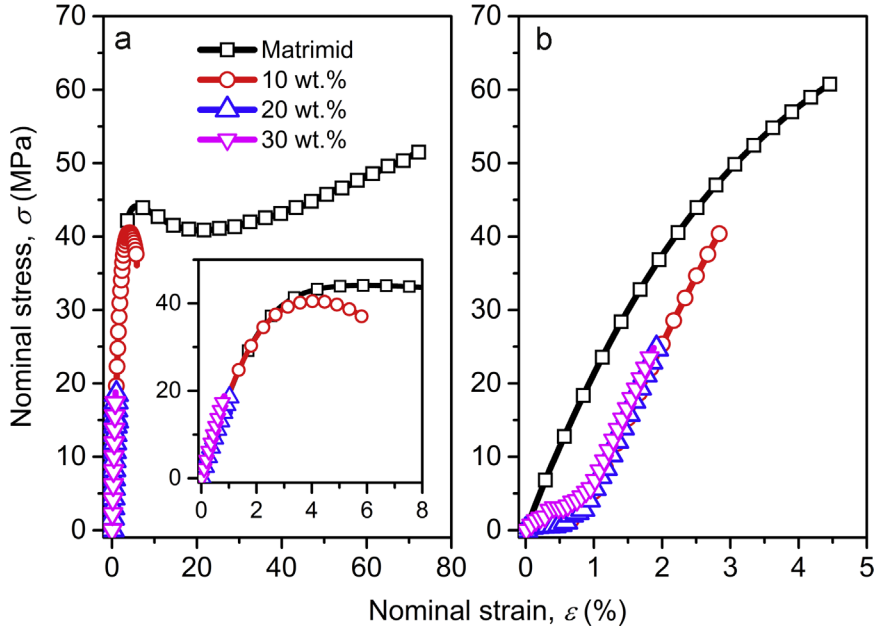

Fig. 9. Representative nominal stress-strain curves for the ZIF-8/Matrimid MMMs under uniaxial tension: (a) unannealed and (b) after annealing at 180 °C in vacuum. The inset shows small strain region, where linear elastic, yielding and plastic deformation (strain hardening) are apparent for unannealed membranes.

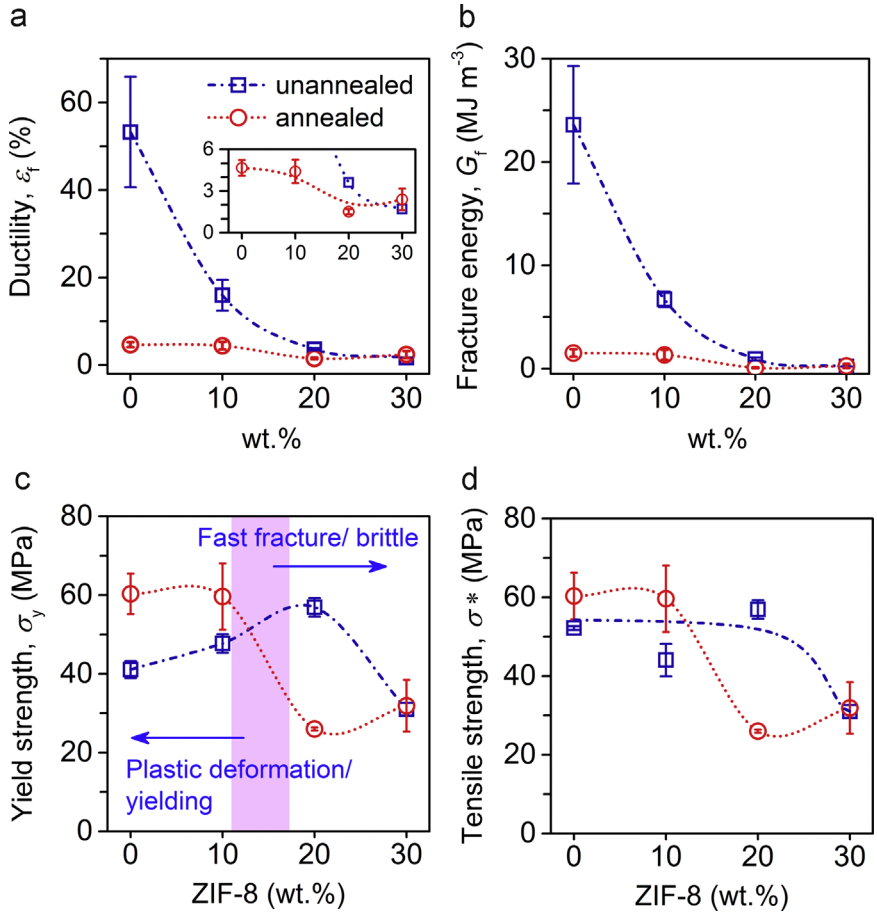

Fig. 10. Mechanical properties derived from the nominal stress-strain plots (Fig. 9) against ZIF-8 wt% loading and annealing condition. (a) Ductility, corresponding to the elongation-to-failure (%), (b) fracture energy, (c) yield strength, and (d) tensile strength. Each standard deviation was derived from three test pieces. The dotted lines serve as guides for the eye.

the neat Matrimid when exceeding 20 wt% loading. Below ~10 wt%, however, we discovered that the strengths of neat Matrimid can be improved by annealing. While the trend observed in the annealed nanocomposites are less systematic (challenging to measure accurately due to fast fracture), the embrittled membranes after annealing show matching values of σ_y and σ^* since the initiation of plastic yielding do coincide with the point of fracture.

3.5. *Practical implications of current findings to the future trends of MOF-based MMMs developed for membrane separation applications*

Given that the vast majority of MOF-based mixed-matrix membranes (MMMs) are in fact developed with gas separations in mind [6,52,73], it is now timely to elucidate how the mechanical properties and viscoelastic information established in this work could offer new insights to the underpinning functional performance of MMMs incorporating MOF fillers. Importantly, the role of this work is to guide future rational design of next generation membranes to yield an optimal combination of mechanical resilience and separation characteristics. Indeed latest review articles have already recognised that there is a "gap" in the literature [2,5,40], correlating the aforementioned factors to the real-world industrial performance of MOF-based MMMs. As a matter of fact, the focus of the great majority of work on MOF-based MMMs concerned the (positive) influence of MOF fillers towards separation performance, *vis-à-vis* neat polymer membranes [6,42,74]. Summarised below are the key practical implications of the current work.

First, we made the important discovery that the presence of residual solvents affecting the overall permeability of MMMs can be unambiguously pinpointed by characterising its viscoelastic response. Specifically, we show how entrapped solvents in membranes account for the relaxation anomalies highlighted in Fig. 7(a, c). Despite the fact that the drying temperature was set to the boiling point of the solvent, we demonstrate that the solvent was not fully removed from the membranes, although this will only be evident when the membranes are subjected to cyclic-loading mechanical tests *via* dynamic mechanical analysis (DMA). By comparison, it should be noted that quasi-static techniques are insensitive to these effects, for example the application of conventional tensile testing on membranes [46,49] cannot reveal such an intrinsic phenomenon associated with residual solvents. By means of DMA, however, strain energy storage and dissipation of membranes are rendered unstable (near T_g) due to occluded solvents, which can be perceived as a 'dampener' interfering with the polymer's attempt to retain or dissipate energy (quantified by E' and E'') under a coupled thermal and cyclic mechanical loading. In the light of this, we propose that the viscoelastic anomalies elucidated above will be prominent for many other MMM systems built from 'glassy' polymeric matrices (T_g > room temperature (RT)), *e.g.* polybenzimidazole (PBI) [43], polyacrylonitrile (PAN) [40], polyethersulfone (PES), and a wide variety of polyimides (Ultem, 6FDA-DAM, etc) [75]. Significantly, here the universal methodology we proposed using DMA is extremely powerful and it could be adopted to future study a broad family of MMMs, including neat polymers and conventional membranes, independent of the type of solvents employed for processing.

Second, we confirmed the efficacy of employing nanoindentation as a viable micromechanical approach to determine the surface and sub-surface (~2 μm) Young's modulus and hardness behaviour of MMMs, featuring a thickness of an order of 10–100 s of micrometres. We show that the variation of mechanical properties can be relatively small for the ZIF-8/Matrimid MMMs ($\Delta E < 0.5$ GPa, $\Delta H < 50$ MPa), but remains discernible. Both properties E and H also scale reasonably well in accordance to the simple Reuss (inversed) Rule of Mixtures [61,65], by assuming an idealised particulate-based filler dispersion in a continuous matrix. Furthermore, because nanoindentation measurements signify the localised fine-scale mechanical characteristics, the corresponding standard deviations (Figs. S7, S8) provide an additional quality indicator about the homogeneity of nanoparticle dispersion at the top surface of membrane. Interestingly, we have witnessed that by combining a stiffer matrix (majority of glassy polymers) with a relatively compliant MOF as filler phase [76] will effectively reduce the elastic moduli of the resultant nanocomposite; but there might be an opposing trend in hardness, for the latter is dictated by the relative magnitude of the hardnesses [34] of the composite constituents. Informed by these outcomes, it can be projected that MMMs made from 'rubbery' polymer matrices (*e.g.* polyurethanes (PUR), polydimethylsiloxane (PDMS), polyisobutylene (PIB)), all of which with a T_g < RT and typical E values of the order of 10–100s MPa [76] can gain improvements in both the stiffness and hardness properties with increasing MOF wt%.

Third, it is essential to highlight that annealing of Matrimid (Fig. 10a, b) is detrimental to its overall ductility (reducing stretchability and bendability), thus leading to a substantial fall in damage tolerance and mechanical resilience (toughness). Likewise, unannealed membranes show a rapid decline in ductility and toughness due to nanoparticle inclusion, which can be explained from the introduction of microscopic stress raisers in an otherwise undisrupted polyimide matrix (Fig. 2). The impact on mechanical strengths, however, is far more complicated. Prior to annealing, there is evidence of improvement in yield and tensile strengths as a function of ZIF-8 inclusion of up to *ca.* 20 wt% loading, beyond which it is likely that nanoparticle aggregation triggers premature membrane cracking and brittle fractures. Nominally, annealing resulted in improved strength of the membranes with up to ~10 wt% nanoparticle loading, before the onset of brittle failure linked to reduced ductility (Fig. 10(a) inset). Our findings demonstrate that additional emphasis *must* be given to the characterisation of material toughness [77], especially from the viewpoint of ductility and fracture energy. To reach practical engineering applications, it is therefore no longer sufficient to consider only elastic modulus and tensile strengths [40,49] to adequately assess the overall mechanical performance of mixed-matrix membranes. Noteworthy, this precise need has also recently been recognised in the emergent field of organic solar cells [78], whose structural requirements (of thin films and coatings) are reminiscent to the mechanical challenges facing MMMs.

Fourth, we may gain useful insights by considering the mechanical properties information presented alongside recently reported gas permeation and selectivity data of ZIF-8/Matrimid MMMs [48], corresponding to the (annealed) membranes engaged in this study. Fig. 11 summarises the selectivity *vs.* mechanical behaviour relationships, suggesting that the optimal ZIF-8/Matrimid nanocomposite membrane may well contain up to ~10 wt% ZIF-8 nanoparticles, and is preferably annealed to maximise selectivity against CO_2, CH_4 and H_2. From the microstructural perspective, it can be seen in Fig. 2(b) that the 10 wt% blend of ZIF-8/Matrimid is uniform, while XRD characterisation had determined distinctive Bragg peaks (Figs. S4, S5) matching that of the ZIF-8 filler, corroborating its crystallinity and intrinsic porosity.

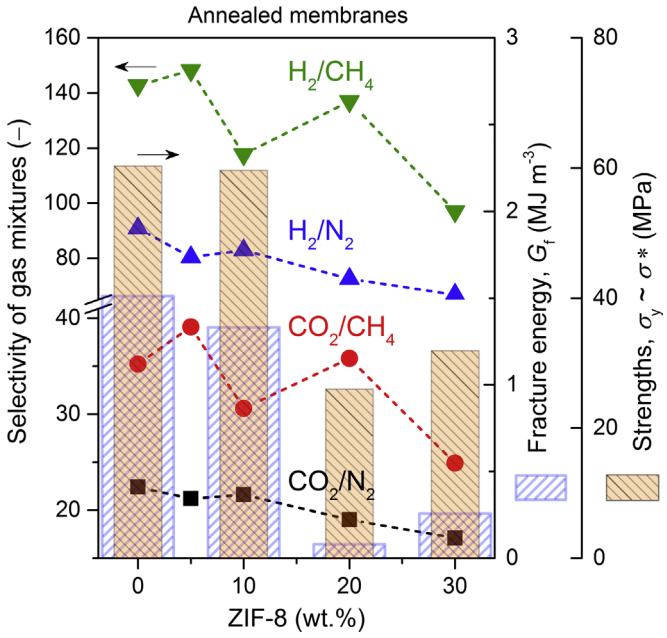

Fig. 11. Comparison of the gas selectivity data of ZIF-8/Matrimid nanocomposite reported by Song *et al.* [48], derived from pure gas permeation properties of annealed membranes. The mechanical properties of annealed membranes measured in this work, especially fracture energy and strengths (mean values), are plotted alongside the selectivity data to highlight the common downward trend as a function of nanoparticle wt% loading; the dotted lines are guides for the eye. Note that during brittle fracture of annealed samples, tensile strengths are approximated by yield strengths due to the limited ductility.

Moreover, viscoelastic analysis showed that the 10 wt% annealed membrane is thermo-mechanically stable under an elastic deformation, extending to a relatively high temperature of ~300 °C (Fig. 7d). When subjected to a large tensile deformation, we established that the 10 wt% annealed membrane retains a respectable level of damage tolerance and mechanical robustness, without compromising its toughness relative to (annealed) neat Matrimid (Fig. 11), rendering us to recommend the application of up to 10 wt% annealed membrane for prospective technological applications. It is worth highlighting that recent exemplars of MMMs, such as the 15 wt% ZIF-90/6FDA-DAM [75] features major enhancements of CO_2 permeability and CO_2/CH_4 selectivity performance; here the matrix termed 6FDA-DAM is a glassy polyimide akin to Matrimid, but the former is appreciably more permeable (higher flux). Yet the corresponding thermo-mechanical performance of the ZIF-90/6FDA-DAM system has not been considered to date.

Finally, while the advent of MOF-based MMMs represents an improvement to the performance of many polymeric membranes, there is an underlying trade-off between separation performance and mechanical robustness, which industrial practitioners will have to rationalise based on the data such as those we have reported in this study. Alas, detailed mechanical properties information like this is still scarce, and might be system specific depending upon the MOF/polymer combination considered. Follow-on studies in the fashion of the current proposed methodology thus will be fundamental to build up a larger picture. Ultimately, if MOF-based MMM membranes are to be successful in real-world engineering applications, the qualitative and quantitative determination methodology of the thermo-mechanical properties of membranes needs to be initiated and developed at this critical stage. In the light of this, it is imperative that we discuss our findings in the wider context of current industrial practices, such as gas separation and pervaporation, due to the fact that the literature is abundant with examples of MOF-based MMMs

developed for these applications, albeit limited at lab-scales, some showing high potential of eventual large-scale industrial utilisation.

Commercial polymer membranes are currently employed in less rigorous gas separation industrial processes, such as hydrogen separation and CO_2/CH_4 separation to afford natural gas purification [40]. Typical exposure conditions for industrial gas separation involving polymeric membranes operates at temperatures of 100–200 °C (depending on the gas) [79] and pressures of *ca.* 10–60 bars (inlet pressure of compressed gas) [80]. Our DMA results proved that Matrimid-based membranes (high T_g) containing ZIF-8 are stable up to temperatures of 300 °C, which makes it a viable industrial candidate for gas separation. We further demonstrated that the ZIF-8/Matrimid membranes are capable of withstanding stresses in the range of up to 60 MPa (depending on ZIF-8 nanoparticle loadings), which is important as these membranes will need to be operable at high pressures that will inevitably induce biaxial deformations (caused by pressure-differential force of the fluids/gases). For high-throughput industrial installations [81], polymeric membranes are typically stacked on top of one another within a cylindrical or ceramic module, offering additional structural support to the membranes while enhancing separation performance by subjecting the feed stock to multiple separation cycles. The nominal viability of a standalone MOF-based membrane successfully studied in a small-scale lab setting could be translated into up-scaled industrial setting, where a combination of multiple membranes stacked in a spiral-wound module [82] may be used (instead of one single membrane for the entire process). There are a few commercial gas separation polymeric systems found on the market that were designed based on this operational concept. Likewise, this configuration applies to commercial pervaporation systems utilising polymeric membranes, where operational temperature ranges are *ca.* 60–150 °C, depending on the solvent mixture used, and the pressures involved are significantly smaller (~few kPa) [83]. These temperature and pressure ranges lie within the range of contemporary MOF-based membranes such as ZIF-8/Matrimid. Additionally, future assessments of mechanical resilience and stability of MMMs should consider also hazards associated with ageing effects, long-term thermo-mechanical degradation and moisture tolerance, amongst others.

4. Conclusions

This work represents the first systematic mechanical characterisation study of a prototypical MOF/Polymer mixed-matrix membrane material, focused on the ZIF-8/Matrimid® nanocomposite system. We have investigated the quasi-static nanoindentation behaviour, temperature-dependent dynamic properties, and large-strain deformation beyond the elastic limit. The objective was to gain new insights of the effects of ZIF-8 nanoparticle inclusions on the mechanical properties and the viscoelastic response of free-standing membranes, which have been developed for emergent gas separation applications.

It was confirmed that the dispersion and encapsulation of ZIF-8 within Matrimid, obtained *via* the colloidal solution mixing technique [48], was uniform and overall homogeneous. Though well dispersed, we established that the addition of ZIF-8 nanoparticles (> 10–15 wt%) to the nanocomposite is detrimental towards mechanical properties of such thin membranes, particularly the ductility, toughness, and tensile strength, making them highly susceptible to cracking by (brittle) fast fracture. This trend is even more pronounced for annealed membranes, in which further embrittlement of the polyimide matrix phase has occurred.

While there are only subtle changes to the viscoelastic properties with the addition of ZIF-8 nanoparticles, major fluctuations associated with residual solvents in cured MMMs have been established near the glass transition temperature (T_g). We demonstrate that DMA is an extremely powerful technique, whose usage should be broadened in the field of MMM research to enable not only the determination of T_g, but also to address evolution of dynamical mechanical behaviour, basic energy dissipation mechanisms, such as to pinpoint the presence of occluded solvents impacting membrane permeability and selectivity.

As per previous work [48] reporting enhancement of gas separation behaviour of ZIF-8/Matrimid nanocomposites, it was established in this study that while the addition of ZIF-8 nanoparticles and annealing are beneficial towards gas selectivity, we show that this is not always the case for certain mechanical properties. Specifically, mechanical degradation in terms of ductility and toughness can be substantial post annealing, thus weakening its structural robustness making material less suitable for practical use.

It is envisaged that the structure-property relationships between MOF nanoparticles and polymer matrix membranes developed in this work, together with the mechanical characterisation methodologies elucidated here will be pertinent to many combinations of MOF-polymer based systems, comprising either a glassy or a rubbery matrix targeting a wide range of emergent membrane technologies. Work is certainly warranted to further establish whether the proposed structure-property correlation is applicable to understand the performance of a broad combination of MMMs.

Acknowledgements

E.M. Mahdi would like to thank Yayasan Khazanah for DPhil scholarship that made this work possible. We acknowledge the Royal Society Research Grants (RG140296) for equipment funding. The authors are grateful to Mr. V.T. Dickinson at Huntsman Advanced Materials (Europe) for provision of the Matrimid® samples. The authors would like to thank Mr. S. Ying and Prof. A.M. Korsunsky for providing access to the Scanning Electron Microscope facilities (MBLEM Laboratory at Oxford, EU FP7 Project iSTRESS (604646)), and to Prof. H. Bhaskaran and Dr. M. Pacios-Pujadó for access to MFP-3D Asylum Research AFM facility, and to Prof. Steve Roberts and Dr. David Armstrong for access to the nanoindentation facilities at Oxford Materials. We are grateful to the ISIS Rutherford Appleton Laboratory, especially Dr. Marek Jura and Dr. Gavin Stenning at R53 Materials Characterisation Laboratory, and Dr. James Taylor at R79 Hydrogen and Catalysis Laboratory for providing access to XRD and spectrometers. We would like to acknowledge the provision of advanced materials characterisation facilities by the Research Complex at Harwell (RCaH), Rutherford Appleton Laboratory, Oxfordshire.

Appendix A. Supplementary material

Supplementary data associated with this article can be found in the online version at http://dx.doi.org/10.1016/j.memsci.2015.09.066.

References

[1] M.M. Pendergast, E.M.V. Hoek, A review of water treatment membrane nanotechnologies, Energy Environ. Sci. 4 (2011) 1946–1971.
[2] D.F. Sanders, Z.P. Smith, R. Guo, L.M. Robeson, J.E. McGrath, D.R. Paul, B. D. Freeman, Energy-efficient polymeric gas separation membranes for a sustainable future: A review, Polymer 54 (2013) 4729–4761.
[3] R.D. Noble, Perspectives on mixed matrix membranes, J. Membr. Sci. 378 (2011) 393–397.

[4] M.G. Buonomenna, J. Bae, Membrane processes and renewable energies, Renew. Sust. Energ. Rev 43 (2015) 1343–1398.
[5] Y. Zhang, J. Sunarso, S. Liu, R. Wang, Current status and development of membranes for CO_2/CH_4 separation: A review, Int. J. Greenh. Gas Control 12 (2013) 84–107.
[6] N. Du, H.B. Park, M.M. Dal-Cin, M.D. Guiver, Advances in high permeability polymeric membrane materials for CO2 separations, Energy Environ. Sci. 5 (2012) 7306–7322.
[7] X.S. Feng, R.Y.M. Huang, Liquid separation by membrane pervaporation: A review, Ind. Eng. Chem. Res. 36 (1997) 1048–1066.
[8] S.S. Shenvi, A.M. Isloor, A.F. Ismail, A review on RO membrane technology: Developments and challenges, Desalination (2015).
[9] Y. Baek, C. Kim, D.K. Seo, T. Kim, J.S. Lee, Y.H. Kim, K.H. Ahn, S.S. Bae, S.C. Lee, J. Lim, K. Lee, J. Yoon, High performance and antifouling vertically aligned carbon nanotube membrane for water purification, J. Membr. Sci. 460 (2014) 171–177.
[10] A. Collier, H. Wang, X. Ziyuan, J. Zhang, D. Wilkinson, Degradation of polymer electrolyte membranes, Int. J. Hydrogen Energy 31 (2006) 1838–1854.
[11] M. Inaba, T. Kinumoto, M. Kiriake, R. Umebayashi, A. Tasaka, Z. Ogumi, Gas crossover and membrane degradation in polymer electrolyte fuel cells, Electrochim. Acta 51 (2006) 5746–5753.
[12] B. Wu, M. Zhao, W. Shi, W. Liu, J. Liu, D. Xing, Y. Yao, Z. Hou, P. Ming, J. Gu, Z. Zou, The degradation study of Nafion/PTFE composite membrane in PEM fuel cell under accelerated stress tests, Int. J. Hydrogen Energy 39 (2014) 14381–14390.
[13] C.H. Worthley, K.T. Constantopoulos, M. Ginic-Markovic, R.J. Pillar, J. G. Matisons, S. Clarke, Surface modification of commercial cellulose acetate membranes using surface-initiated polymerization of 2-hydroxyethyl methacrylate to improve membrane surface biofouling resistance, J. Membr. Sci., 385-386 (2011) 30–39.
[14] Z.Q. Jiang, Z.J. Jiang, Plasma techniques for the fabrication of polymer electrolyte membranes for fuel cells, J. Membr. Sci. 456 (2014) 85–106.
[15] C.-H. Tsai, C.-C. Wang, C.-Y. Chang, C.-H. Lin, Y.W. Chen-Yang, Enhancing performance of Nafion®-based PEMFC by 1-D channel metal-organic frameworks as PEM filler, Int. J. Hydrogen Energy 39 (2014) 15696–15705.
[16] S. Xia, M. Ni, Preparation of poly(vinylidene fluoride) membranes with graphene oxide addition for natural organic matter removal, J. Membr. Sci. 473 (2015) 54–62.
[17] N. Ghaemi, S.S. Madaeni, P. Daraei, H. Rajabi, S. Zinadini, A. Alizadeh, R. Heydari, M. Beygzadeh, S. Ghouzivand, Polyethersulfone membrane enhanced with iron oxide nanoparticles for copper removal from water: Application of new functionalized Fe_3O_4 nanoparticles, Chem. Eng. J. 263 (2015) 101–112.
[18] E. Ameri, M. Sadeghi, N. Zarei, A. Pournaghshband, Enhancement of the gas separation properties of polyurethane membranes by alumina nanoparticles, J. Membr. Sci. 479 (2015) 11–19.
[19] C.-W. Liew, S. Ramesh, A.K. Arof, Characterization of ionic liquid added poly (vinyl alcohol)-based proton conducting polymer electrolytes and electrochemical studies on the supercapacitors, Int. J. Hydrogen Energy 40 (2015) 852–862.
[20] Y. Tang, A. Kusoglu, A.M. Karlsson, M.H. Santare, S. Cleghorn, W.B. Johnson, Mechanical properties of a reinforced composite polymer electrolyte membrane and its simulated performance in PEM fuel cells, J. Power Sources 175 (2008) 817–825.
[21] G.D. Vilakati, E.M.V. Hoek, B.B. Mamba, Probing the mechanical and thermal properties of polysulfone membranes modified with synthetic and natural polymer additives, Polymer Test. 34 (2014) 202–210.
[22] S. Thampi, V. Muthuvijayan, R. Parameswaran, Mechanical characterization of high-performance graphene oxide incorporated aligned fibroporous poly (carbonate urethane) membrane for potential biomedical applications, J. Appl. Polym. Sci. 132 (2015) 41809.
[23] R. Pucciariello, M. D'Auria, V. Villani, G. Giammarino, G. Gorrasi, G. Shulga, Lignin/Poly(ε-Caprolactone) Blends with Tuneable Mechanical Properties Prepared by High Energy Ball-Milling, J. Polym. Environ. 18 (2010) 326–334.
[24] R. Mahajan, W.J. Koros, Factors controlling successful formation of mixed-matrix gas separation materials, Ind. Eng. Chem. Res. 39 (2000) 2692–2696.
[25] D.R. Paul, L.M. Robeson, Polymer nanotechnology: Nanocomposites, Polymer 49 (2008) 3187–3204.
[26] J. Zhu, W. Cao, M. Yue, Y. Hou, J. Han, M. Yang, Strong and stiff aramid nanofiber/carbon nanotube nanocomposites, ACS Nano 9 (2015) 2489–2501.
[27] H. Kim, A.A. Abdala, C.W. Macosko, Graphene/polymer nanocomposites, Macromolecules 43 (2010) 6515–6530.
[28] S.T. Meek, J.A. Greathouse, M.D. Allendorf, Metal–organic frameworks: a rapidly growing class of versatile nanoporous materials, Adv. Mater. 23 (2011) 249–267.
[29] J.C. Tan, B. Civalleri, Metal–organic frameworks and hybrid materials: from fundamentals to applications, CrystEngComm 17 (2015) 197–198.
[30] S. Kitagawa, R. Kitaura, S. Noro, Functional porous coordination polymers, Angew. Chem. Int. Ed. 43 (2004) 2334–2375.
[31] H. Furukawa, K.E. Cordova, M. O'Keeffe, O.M. Yaghi, The chemistry and applications of metal–organic frameworks, Science 341 (2013) 974–986.
[32] H.C. Zhou, J.R. Long, O.M. Yaghi, Introduction to metal-organic frameworks, Chem. Rev. 112 (2012) 673–674.
[33] R. Banerjee, A. Phan, B. Wang, C. Knobler, H. Furukawa, M. O'Keeffe, O. M. Yaghi, High-throughput synthesis of zeolitic imidazolate frameworks and application to CO_2 capture, Science 319 (2008) 939–943.
[34] J.C. Tan, T.D. Bennett, A.K. Cheetham, Chemical structure, network topology, and porosity effects on the mechanical properties of zeolitic imidazolate frameworks, Proc. Natl. Acad. Sci. USA 107 (2010) 9938–9943.
[35] J.C. Tan, B. Civalleri, C.C. Lin, L. Valenzano, R. Galvelis, P.F. Chen, T.D. Bennett, C. Mellot-Draznieks, C.M. Zicovich-Wilson, A.K. Cheetham, Exceptionally low shear modulus in a prototypical imidazole-based metal–organic framework, Phys. Rev. Lett. 108 (2012) 095502.
[36] T.D. Bennett, D.A. Keen, J.C. Tan, E.R. Barney, A.L. Goodwin, A.K. Cheetham, Thermal amorphization of zeolitic imidazolate frameworks, Angew. Chem. Int. Ed. 50 (2011) 3067–3071.
[37] M.R. Ryder, B. Civalleri, T.D. Bennett, S. Henke, S. Rudić, G. Cinque, F. Fernandez-Alonso, J.C. Tan, Identifying the role of terahertz vibrations in metal-organic frameworks: from gate-opening phenomenon to shear-driven structural destabilization, Phys. Rev. Lett. 113 (2014) 215502.
[38] J.C. Tan, B. Civalleri, A. Erba, E. Albanese, Quantum mechanical predictions to elucidate the anisotropic elastic properties of zeolitic imidazolate frameworks: ZIF-4 vs. ZIF-zni, CrystEngComm 17 (2015) 375–382.
[39] M.R. Ryder, J.C. Tan, Nanoporous metal–organic framework materials for smart applications, Mater. Sci. Tech 30 (2014) 1598–1612.
[40] G.X. Dong, H.Y. Li, V.K. Chen, Challenges and opportunities for mixed-matrix membranes for gas separation, J. Mater. Chem. A 1 (2013) 4610–4630.
[41] A.W. Thornton, D. Dubbeldam, M.S. Liu, B.P. Ladewig, A.J. Hill, M.R. Hill, Feasibility of zeolitic imidazolate framework membranes for clean energy applications, Energy Environ. Sci. 5 (2012) 7637–7646.
[42] H.B.T. Jeazet, C. Staudt, C. Janiak, Metal-organic frameworks in mixed-matrix membranes for gas separation, Dalton Trans. 41 (2012) 14003–14027.
[43] T.X. Yang, G.M. Shi, T.S. Chung, Symmetric and Asymmetric Zeolitic Imidazolate Frameworks (ZIFs)/Polybenzimidazole (PBI) Nanocomposite Membranes for Hydrogen Purification at High Temperatures, Adv. Energy Mater. 2 (2012) 1358–1367.
[44] S.N. Liu, G.P. Liu, X.H. Zhao, W.Q. Jin, Hydrophobic-ZIF-71 filled PEBA mixed matrix membranes for recovery of biobutanol via pervaporation, J. Membr. Sci. 446 (2013) 181–188.
[45] S.-L. Li, Q. Xu, Metal-organic frameworks as platforms for clean energy, Energy Environ. Sci. 6 (2013) 1656–1683.
[46] S.N. Wijenayake, N.P. Panapitiya, S.H. Versteeg, C.N. Nguyen, S. Goel, K. J. Balkus, I.H. Musselman, J.P. Ferraris, Surface cross-linking of ZIF-8/polyimide mixed matrix membranes (MMMs) for gas separation, Ind. Eng. Chem. Res. 52 (2013) 6991–7001.
[47] F. Mammeri, E.L. Bourhis, L. Rozes, C. Sanchez, Mechanical properties of hybrid organic–inorganic materials, J. Mater. Chem. 15 (2005) 3787.
[48] Q. Song, S.K. Nataraj, M.V. Roussenova, J.C. Tan, D.J. Hughes, W. Li, P. Bourgoin, M.A. Alam, A.K. Cheetham, S.A. Al-Muhtaseb, E. Sivaniah, Zeolitic imidazolate framework (ZIF-8) based polymer nanocomposite membranes for gas separation, Energy Environ. Sci. 5 (2012) 8359-r.
[49] M.J.C. Ordoñez, K.J. Balkus, J.P. Ferraris, I.H. Musselman, Molecular sieving realized with ZIF-8/Matrimid® mixed-matrix membranes, J. Membr. Sci. 361 (2010) 28–37.
[50] S.J. Smith, B.P. Ladewig, A.J. Hill, C.H. Lau, M.R. Hill, Post-synthetic Ti Exchanged UiO-66 metal–organic frameworks that deliver exceptional gas permeability in mixed matrix membranes, Sci. Rep. 5 (2015) 7823.
[51] T. Rodenas, I. Luz, G. Prieto, B. Seoane, H. Miro, A. Corma, F. Kapteijn, I.X.F. X. Llabres, J. Gascon, Metal-organic framework nanosheets in polymer composite materials for gas separation, Nat. Mater. 14 (2015) 48–55.
[52] M. Rezakazemi, A. Ebadi Amooghin, M.M. Montazer-Rahmati, A.F. Ismail, T. Matsuura, State-of-the-art membrane based CO_2 separation using mixed matrix membranes (MMMs): an overview on current status and future directions, Prog. Polym. Sci. 39 (2014) 817–861.
[53] S.M. Janosch Cravillon, Sven-Jare Lohmeier, Armin Feldhoff, Klaus Huber, Michael Wiebcke, Rapid room-temperature synthesis and characterization of nanocrystals of a prototypical zeolitic imidazolate framework, Chem. Mater. 21 (2009) 1410–1412.
[54] J. Cravillon, R. Nayuk, S. Springer, A. Feldhoff, K. Huber, M. Wiebcke, Controlling zeolitic imidazolate framework nano- and microcrystal formation: insight into crystal growth by time-resolved in situ static light scattering, Chem. Mater. 23 (2011) 2130–2141.
[55] D. Ballestero, R. Juan, A. Ibarra, C. Gomez-Gimenez, C. Ruiz, B. Rubio, M. T. Izquierdo, Effect of thermal treatments on the morphology, chemical state and lattice structure of gold nanoparticles deposited onto carbon structured monoliths, Colloids Surf. A 468 (2015) 140–150.
[56] A.C. Comer, D.S. Kalika, B.W. Rowe, B.D. Freeman, D.R. Paul, Dynamic relaxation characteristics of Matrimid® polyimide, Polymer 50 (2009) 891–897.
[57] W.C. Oliver, G.M. Pharr, An improved technique for determining hardness and elastic modulus using load and displacement sensing indentation experiments, J. Mater. Res. 7 (1992) 1564–1583.
[58] A.M. Díez-Pascual, M.A. Gómez-Fatou, F. Ania, A. Flores, Nanoindentation in polymer nanocomposites, Prog. Mater. Sci. 67 (2015) 1–94.
[59] J.C. Tan, C.A. Merrill, J.B. Orton, A.K. Cheetham, Anisotropic mechanical properties of polymorphic hybrid inorganic-organic framework materials with different dimensionalities, Acta Mater. 57 (2009) 3481–3496.
[60] J.C. Tan, J.D. Furman, A.K. Cheetham, Relating mechanical properties and chemical bonding in an inorganic–organic framework material: a single-crystal nanoindentation study, J. Am. Chem. Soc. 131 (2009) 14252–14254.
[61] D. Hull, T.W. Clyne, An Introduction to Composite Materials, Cambridge University Press, 1996.

[62] N.W. Khun, E.M. Mahdi, S.Q. Ying, T. Sui, A.M. Korsunsky, J.C. Tan, Fine-scale tribological performance of zeolitic imidazolate framework (ZIF-8) based polymer nanocomposite membranes, APL Mater. 2 (2014) 124101.
[63] S. Hwang, W.S. Chi, S.J. Lee, S.H. Im, J.H. Kim, J. Kim, Hollow ZIF-8 nanoparticles improve the permeability of mixed matrix membranes for CO_2/CH_4 gas separation, J. Membr. Sci. 480 (2015) 11–19.
[64] S.J.K. Jensen, T.H. Tang, I.G. Csizmadia, Hydrogen-bonding ability of a methyl group, J. Phys. Chem. A 107 (2003) 8975–8979.
[65] R. Lakes, Viscoelastic Materials, Cambridge University Press, 2009.
[66] M.C. Righetti, A. Boggioni, M. Laus, D. Antonioli, K. Sparnacci, L. Boarino, Thermal and mechanical properties of PES/PTFE composites and nanocomposites, J. Appl. Polym. Sci. 130 (2013) 3624–3633.
[67] S. Liu, R. Ananthoji, S. Han, B. Knudsen, X. Li, L. Wojtas, J. Massing, C. V. Gauthier, J.P. Harmon, Poly(methyl methacrylate) composites of copper-4,4′-trimethylenedipyridine, New J. Chem. 36 (2012) 1449.
[68] T. Wan, T. Du, B.A. Wang, W. Zeng, M. Clifford, Microstructure, crystallization and dynamic mechanical properties of polyamide/clay nanocomposites after melt-state annealing, Polym. Compos. 33 (2012) 2271–2276.
[69] A.C. Comer, C.P. Ribeiro, B.D. Freeman, S. Kalakkunnath, D.S. Kalika, Dynamic relaxation characteristics of thermally rearranged aromatic polyimides, Polymer 54 (2013) 891–900.
[70] S.A. Moggach, T.D. Bennett, A.K. Cheetham, The effect of pressure on ZIF-8: increasing pore size with pressure and the formation of a high-pressure phase at 1.47 GPa, Angew. Chem. Int. Ed. 48 (2009) 7087–7089.
[71] C. Casado-Coterillo, J. Soto, M.T. Jimaré, S. Valencia, A. Corma, C. Téllez, J. Coronas, Preparation and characterization of ITQ-29/polysulfone mixed-matrix membranes for gas separation: effect of zeolite composition and crystal size, Chem. Eng. Sci. 73 (2012) 116–122.
[72] J.C. Tan, T.W. Clyne, Ferrous fibre network materials for jet noise reduction in aeroengines Part II: thermo-mechanical stability, Adv. Eng. Mater. 10 (2008) 201–209.
[73] B. Zornoza, C. Tellez, J. Coronas, J. Gascon, F. Kapteijn, Metal organic framework based mixed matrix membranes: an increasingly important field of research with a large application potential, Microporous Mesoporous Mater. 166 (2013) 67–78.
[74] T.H. Bae, J.R. Long, CO_2/N_2 separations with mixed-matrix membranes containing Mg_2(dobdc) nanocrystals, Energy Environ. Sci. 6 (2013) 3565.
[75] T.H. Bae, J.S. Lee, W.L. Qiu, W.J. Koros, C.W. Jones, S. Nair, A. High-Performance Gas-Separation, Membrane containing submicrometer-sized metal-organic framework crystals, Angew. Chem. Int. Ed. 49 (2010) 9863–9866.
[76] J.C. Tan, A.K. Cheetham, Mechanical properties of hybrid inorganic–organic framework materials: establishing fundamental structure–property relationships, Chem. Soc. Rev. 40 (2011) 1059–1080.
[77] R.O. Ritchie, The conflicts between strength and toughness, Nat. Mater. 10 (2011) 817–822.
[78] S. Savagatrup, A.D. Printz, T.F. O'Connor, A.V. Zaretski, D. Rodriquez, E. J. Sawyer, K.M. Rajan, R.I. Acosta, S.E. Root, D.J. Lipomi, Mechanical degradation and stability of organic solar cells: molecular and microstructural determinants, Energy Environ. Sci. 8 (2015) 55–80.
[79] M.G. De Angelis, G.C. Sarti, Gas sorption and permeation in mixed matrix membranes based on glassy polymers and silica nanoparticles, Curr. Opin. Chem. Eng. 1 (2012) 148–155.
[80] J. Caro, M.O.F. Are, membranes better in gas separation than those made of zeolites? Curr. Opin. Chem. Eng. 1 (2011) 77–83.
[81] P. Bernardo, E. Drioli, G. Golemme, Membrane gas separation: a review/state of the art, Ind. Eng. Chem. Res. 48 (2009) 4638–4663.
[82] R.W. Baker, Future directions of membrane gas separation technology, Ind. Eng. Chem. Res. 41 (2002) 1393–1411.
[83] D. Hua, Y.K. Ong, Y. Wang, T. Yang, T.-S. Chung, ZIF-90/P84 mixed matrix membranes for pervaporation dehydration of isopropanol, J. Membr. Sci. 453 (2014) 155–167.